A NOVEL PROCEDURE TO DETERMINE THE COHESIVE LAW IN DCB TESTS

Ainhoa Arrese[1], Ana I. Boyano[2], Juan De Gracia[2] and Faustino Mujika[1]

[1,2]Materials+Technologies Group/ Mechanics of Materials

[1,2]Department of Mechanical Engineering

[1]Faculty of Engineering of Gipuzkoa (UPV/EHU), San Sebastián, Spain

[2]Faculty of Engineering of Vitoria-Gasteiz (UPV/EHU), Spain

Email: ainhoa.arrese@ehu.eus,

Keywords: Interlaminar failure, Cohesive zone, DCB test, mode I

ABSTRACT

A novel method is presented for the determination of mode I cohesive law for the characterization of delamination in unidirectional carbon fiber reinforced polymer laminates. The energy release rate as a function of the crack advance is determined based on an analytical approach where the compliance variation of the specimen as crack advances is used in order to obtain the crack length for every pair of load and displacement data. Based on the same analytic approach, the crack tip opening displacement is determined as a function of the equivalent crack advance assuming that the Fracture Process Zone development is analogous to an equivalent crack advance Δa. These measurements are used to compute the Energy Release Rate and crack opening displacement from which a cohesive law is determined by numerical differentiation. This new method provides a simple way to obtain the mode I cohesive law using only the load and displacement data obtained from the testing machine, without any external displacement measurement technique and without any assumption of the form of the cohesive law.

1. INTRODUCTION

Carbon Fibre Reinforced Polymer composites (CFRP) are widely used in advanced structural design, due to their high specific strength. However, their limited resistance to matrix dominated failures makes delamination one of the most concerns in the design of advanced composite structures. Interlaminar cracks, which can initiate at a free edge or at defects from manufacturing, are very difficult to detect and their presence may significantly reduce the global stiffness and compressive strength of the structure. Thus, modeling of the interlaminar behavior is crucial for safe design of an advanced structural component; especially when initiation of cracks is studied. Most numerical and theoretical analyses evaluate the energy release rate based on fracture mechanics approaches. Among the available methods for the investigation of crack propagation by means of finite element codes, the Virtual Crack Closure Technique (VCCT) and the cohesive zone model (CZM) are extensively used [1-6]. VCCT was first formulated by Rybicki and Kanninen [7]. It is computationally simple and it is considered an effective method for determining the energy release rate. Nevertheless, it is not suitable analyzing the delamination growth.

CZM was introduced in the early sixties by Barenblatt [8] and Dugdale [9] and describes the local fracture processes near the crack tips as a gradual phenomenon where the separation takes place across a cohesive zone. It is widely used in the commercial finite element packages due to the applicability for analyzing the fracture of different materials under different load conditions. With CZM, fracture is modeled as a process where a surface in the material first forms a cohesive zone called the fracture process zone (FPZ). The FPZ is later separated into two crack surfaces. In the cohesive zone, the crack surfaces are held together by cohesive tractions.

The general idea is that the fracture process is described by a local stress-relative displacement relation of a fracture process zone (FPZ). This relation is a constitutive law of

the material, named cohesive law. The fracture process zone length (L_{FPZ}) is the distance at the crack plane where the cohesive tractions are acting. Figure 1 illustrates a cohesive model, where the traction is assumed to decrease as the relative displacement of the cohesive surfaces increases. For a critical displacement, the traction is zero and a new crack surface is created.

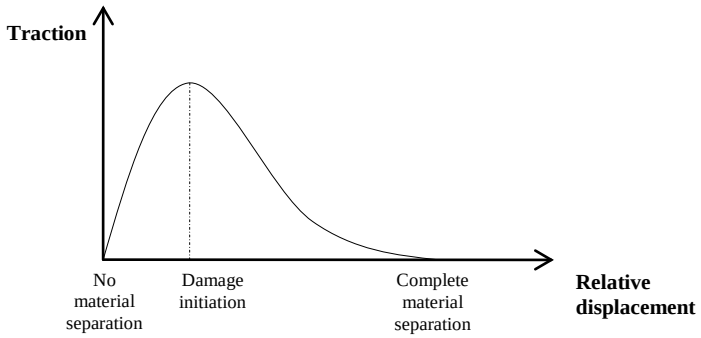

Figure1. General form of a cohesive zone law

The cohesive law plays an important role in the simulation of the fracture behavior of materials [10]. Thus, methods to determine the cohesive law of adhesive layers have been developed by several authors [11- 17] methods to characterize the cohesive law and the fibre bridging law in laminated composites have been developed as well [18 -23].

For carbon fibre reinforced composites, two different delamination processes can be identified: one that takes place at the close proximity of the crack tip with a sub millimeter sized process zone and the other with a large scale process zone related to the fiber bridging effect [21].

In order to determine relative displacements at the crack tip, those methods require the use of external equipment as Digital Image Correlation (DIC) or Linear voltage differential transformer (LVDT) [12,13,15-22]. Experimental difficulties associated with the existing measurement methods have been reported, related to inaccurate results in the measurement of very small crack tip separations [13, 21].

In the present study, a new method to determine the cohesive law in Mode I has been developed. It is based on the determination of the crack length due to the compliance variation of the specimen as crack advances, for every pair of load and displacement data recorded during the test. This method has been validated in a previous study [24]. Therefore, the energy release rate as a function of the crack advance is determined using only the load and displacement data obtained from the testing machine. Based on the same analytic approach, the crack tip opening displacement Δ_n is determined as a function of the equivalent crack advance. Therefore, the energy release rate G can be expressed as a function of Δ_n. Finally, the cohesive law is obtained by numerical differentiation of G with respect to Δ_n .

2. ANALYTIC APPROACH

The J integral, presented by Rice [25] is a path independent contour integral for analysis of cracks can be calculated from the integral:

$$J = \int_c \left(W dy - \boldsymbol{T} \frac{\partial \boldsymbol{u}}{\partial x} \, dc \right) \tag{1}$$

Where c is the counter clockwise integration path, W is the strain energy density, $\boldsymbol{T}$ the traction vector and $\boldsymbol{u}$ the displacement vector. By choosing c close to the crack tip, $\boldsymbol{T}$ is null [11,25,26] and Eq. (1) becomes in:

$$J = \int_C W dy = \int_0^{\Delta_n} \sigma \, d\Delta_n + \int_0^{\Delta_t} \tau \, d\Delta_t \tag{2}$$

where σ, τ, Δ_n and Δ_t are the cohesive normal stress, shear stress, opening and shear displacement at the crack tip, respectively.

Furthermore it is shown that the J-integral is equivalent to Energy Release Rate G for an elastic material [25-29]

$$J = G = \frac{1}{b} \left[\frac{\partial U^*}{\partial a} \right]_P \tag{3}$$

where U^* is the complementary strain energy stored in the body, a is the crack length, b is the width and the subscript P follows the partial derivative convention indicating the load variable is held constant during partial differentiation.

According to Eq. (2) if the relationship among G, Δ_n and Δ_t is known, assuming that G is an exact differential, the cohesive laws can be obtained as

$$\sigma(\Delta_n, \Delta_t) = \frac{\partial G}{\partial \Delta_n} \qquad \tau(\Delta_n, \Delta_t) = \frac{\partial G}{\partial \Delta_t} \tag{4}$$

For a symmetric specimen, symmetrically loaded with a crack advancing along the mid-plane, the crack opening displacement is normal to the crack plane and the crack shear displacement is zero. Then, the cohesive normal stress σ depends only on the normal opening Δ_n [28, 30], being:

$$\sigma(\Delta_n) = \frac{\partial G}{\partial \Delta_n} \tag{5}$$

The double cantilever beam (DCB) test shown in Fig. 2 is the most popular method used to calculate delamination toughness in mode I [31]. In order to achieve pure mode I, a pre-cracked specimen is loaded at one edge by means of bonded blocks or piano hinges. .

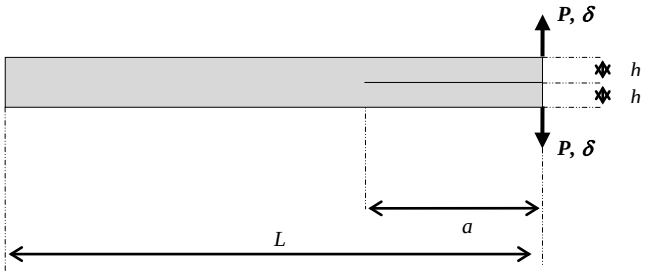

Figure 2: Schematic DCB specimen

Recently, a method to determine G for every pair of load and displacement data during the test has been proposed [24]. By this method the energy release rate is determined without any optical measurement of the crack length, based on a model that simplifies the stress distribution on the uncracked part of the specimen. The crack length is obtained based on the

compliance after having determined the elastic properties of the specimen. Furthermore, large displacements effects are included in a simple manner. In this way, the crack length is determined continuously, and thus a plot of the *R*-curve can be also determined.

Fig. 3 shows the simplified model with distributed forces based on the results of the elastic foundation models presented by different authors [32- 39]. These models present a common shape for the stress distribution ahead of the crack tip, which has been approached to the one caused by two triangular distributed forces q_1 and q_3. The maximum intensities of the distributed loads are q_{10} and q_{30} located at Sections 1 and 3, respectively.

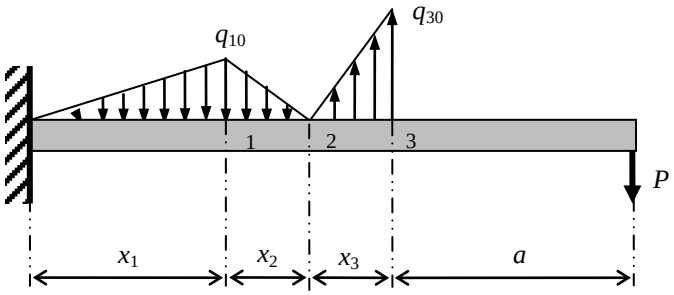

Figure 3: Distributed force along the beam

The displacement of the loading point can be determined applying the Engesser–Castigliano's theorem [40,29], which in the case of shear and bending is given by

$$\delta_i = \left[\frac{\partial U^*}{\partial F_i}\right]_a = \int_L \frac{M}{E_f I}\frac{\partial M}{\partial F_i}dx + \int_L \frac{6}{5}\frac{Q}{G_{13}A}\frac{\partial Q}{\partial F_i}dx \qquad (6)$$

Being F_i an independent applied force; δ_i the displacement of the application point of F_i in the direction of F_i; M is the bending moment; Q is the shear force; E_f is the flexural modulus; $G_{13} = G_{12}$ is the shear modulus, assuming transverse isotropy; I is the second moment of area; A is the cross sectional area.

The derivatives of bending moments and shear forces are obtained applying a vertical unit load at the end section of the clamped beam of Fig. 3. The end point displacement is:

$$\delta = \delta_3 + \theta_3 a + \frac{Pa^3}{3E_f I} + \frac{6Pa}{5AG_{13}} \tag{7}$$

Where the displacement and the bending angle of the section 3 concerning the equivalent crack tip are:

$$\delta_3 = \frac{4P}{k_e}(\beta_4 + \beta_2\, a) \qquad \theta_3 = \frac{P}{12E_f I}(\beta_3 + 3\,\beta_1\, a) \tag{8}$$

Being k_e the tensile stiffness of the elastic foundation $k_e = \frac{2E_3 b}{h}$ where E_3 is the transverse Young's modulus of the material, b is the width and h is the thickness of an adjacent sub-laminate.

The factors β only depend on the dimensions x_1, x_2 and x_3 which do not vary for a given thickness of the specimen [24]. β parameters are:

$$\beta_1 = \frac{x_1^2 + 3x_1x_2 + 4x_1x_3 + 3x_2^2 + 8x_2x_3 + 5x_3^2}{x_1 + 2x_2 + 2x_3}$$

$$\beta_2 = \frac{3}{x_3(x_1 + 2x_2 + 2x_3)}$$

$$\beta_3 = \frac{x_1^2x_3+3x_1x_3^2+3x_1x_2x_3+3x_2^2x_3+6x_2x_3^2+3x_3^3}{x_1+2x_2+2x_3} \tag{9}$$

$$\beta_4 = \frac{x_1 + 2x_2 + 3x_3}{x_3(x_1 + 2x_2 + 2x_3)}$$

x_1, x_2 and x_3 distances were determined in [24] based on the Engesser-Castigliano theorem.

Taking into account Eq. (7), the compliance of DCB specimen can be written as:

$$C = \frac{2\delta}{P} = \frac{2}{3E_f I}a^3 + \frac{2\beta_1}{4E_f I}a^2 + 2\left[\frac{6}{5AG_{13}} + \frac{2\beta_2 h}{bE_3} + \frac{\beta_3}{12E_f I}\right]a + \frac{4\beta_4 h}{bE_3} \tag{10}$$

In order to determine the equivalent crack length, Eq. (10) can be equated to the experimental value computed directly from the measured load–displacement curve. As the crack length is the only unknown quantity, it is obtained by means of an iterative method. This procedure allows obtaining the crack length at any stage of the test where P and δ are evaluated.

Taking into account that $U^* = \frac{P^2}{2}C$ According to Eq (3) and Eq. (10), G is:

$$G = \frac{P^2 a^2}{bE_f I} + \frac{P^2 \beta_1 a}{2bE_f I} + \frac{6P^2}{5bAG_{13}} + \frac{2\beta_2 hP^2}{b^2 E_3} + \frac{\beta_3 P^2}{12bE_f I} \quad (11)$$

In the current approach the Fracture Process Zone (FPZ) development is assumed to be analogous to an equivalent crack advance Δa, related to the compliance variation.

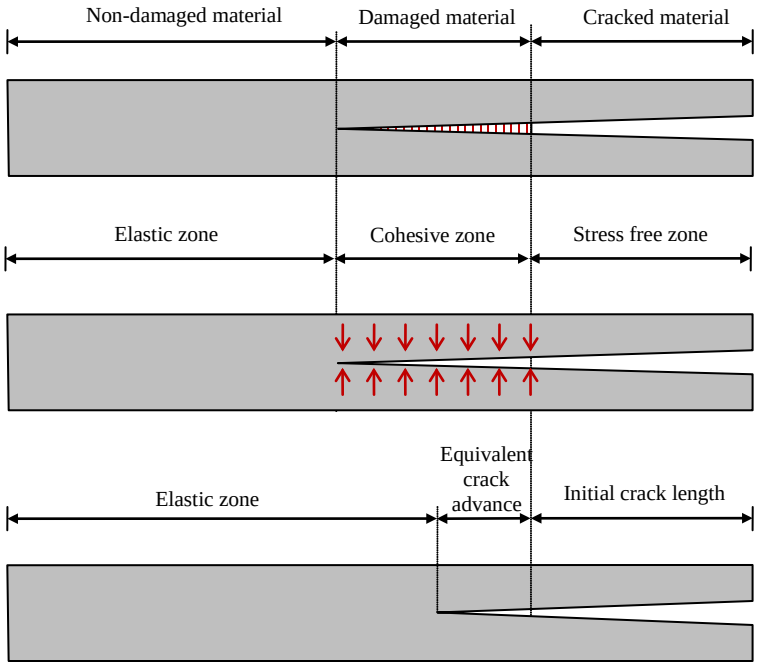

Figure 4: FPZ of a quasi brittle material (top), Cohesive zone model concept (middle) [14] and the equivalent approach proposed in the present work (bottom).

Then, the crack tip opening displacement Δ_n is obtained assuming that the elastic zone of Fig. 4 moves a quantity equal to the equivalent crack advance Δa but without changing the initial crack tip position as it can be seen in Fig 5. Therefore, the initial crack length a_i remains unchanged.

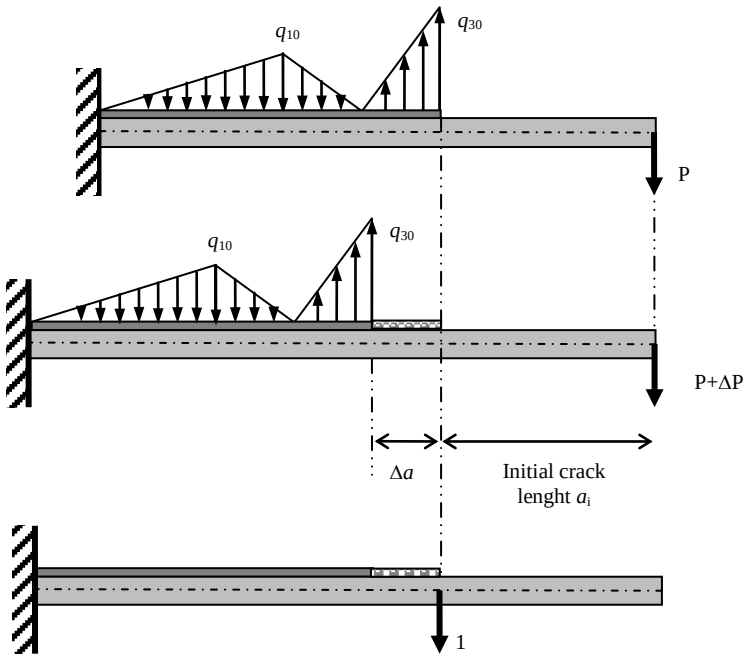

Figure 5: Distributed force along the beam

In order to get the crack tip opening displacement, the unit load method and the Engesser–Castigliano's theorem given in Eq (6) are used applying a unit load at the initial crack tip position in order to get the derivatives of the bending moment and the shear force. The relative opening displacement at the initial crack tip is given by:

$$\Delta_n = 2\delta_3 + 2\theta_3\Delta a + \frac{P}{3E_f I}[-\Delta a^3 + 3\Delta a^2 a] + \frac{12P\Delta a}{5AG_{13}} \qquad (12)$$

Representing the energy release rate with respect to crack opening displacement, according to Eq (5) the cohesive law can be obtained by numerical differentiation. To avoid excessive noise of experimental data, relation G- Δ_n is written as a logistic function with the following form [41]:

$$\frac{G}{G_B} = \left[e^{-\frac{1}{F(\Delta_n)}}\right] \Longrightarrow F(\Delta_n) = -\frac{1}{Ln\left[\frac{G}{G_B}\right]} \qquad (13)$$

G_B is the asymptotic value of the G and $F(\Delta_n)$ a function that is obtained by a first order regional fit using the commercial software *Data curve fit creator Add in V262*[42]. According

to Eq (5) the cohesive law is obtained from the derivative of Eq. (13), replacing the values of the derivative of F(Δ_n) obtained by numerical differentiation.

$$\sigma(\Delta) = \frac{\partial G}{\partial \Delta_n} = G_B \frac{e^{-1/F(\Delta_n)}}{F(\Delta_n)^2} \left[\frac{dF(\Delta_n)}{d\Delta_n}\right] \quad (14)$$

3. EXPERIMENTAL PROCEDURE

3.1. MATERIALS AND APPARATUS

T6T/F593 prepregs provided by Hexcel Composites, with a 50% volume-content of fiber, were used to produce laminates. The plates were manufactured by hot press molding. Sixteen-layered unidirectional laminates, $[0]_{16}$, were made with a Teflon film introduced during the piling up process in order to make the initial crack.

Specimens were cut with a diamond disc saw, being the nominal thickness and width of the specimens 3 and 15 mm, respectively. The edges of the laminate were discarded for the preparation of the specimens. Piano hinges were bonded to the specimens and tests were performed using a universal testing machine MTS-Insight 10 with a load cell of 250 N. In order to avoid the influence of the resin rich area the specimens were precracked in mode II by a ENF test, increasing the cracked length around 5 mm.

3.2. PRELIMINARY TESTS

For obtaining the elastic properties E_f and G_{13}, the procedure based on three-point bending tests at different spans proposed by Mujika [43] was used, resulting in a longitudinal flexural modulus of 116,5 GPa and a shear modulus of 4,4 GPa. Bending tests were done for each specimen in the uncracked zone, at five different spans.

Specimen displacement (δ_{spec}) was determined from load–displacement curves. The experimental displacement (δ_{exp}) is the addition of the specimen displacement and the displacement due to the system compliance.

$$\delta_{exp} = \delta_{spec} + C_s P \longrightarrow \delta_{spec} = \delta_{exp} - C_s P \quad (15)$$

In order to analyze system compliance, a thin steel plate with bonded piano hinges was tested five times as a DCB specimen. As the deformation of the plate is negligible, the slope of the obtained load–displacement curves can be considered to be the effect of the system compliance. The average value obtained for the stiffness of the system was $C_s = 201 \cdot 10^{-5}$ mm/N.

The transverse Young's modulus of the material is E_3=8GPa [24]

C_s includes the compliance effects concerning the different parts of the testing system:

- Piano hinges bonded to the specimen.
- Load cell.
- Testing machine frame.

3.3. DETERMINATION OF THE COHESIVE LAW

An experimental load - displacement curve that corresponds to a specimen named S1 is shown in Fig.6. The following points are marked in the load displacement curve:

- A: Local damage initiation point
- B: The last point of the test
- C: Maximum load point

As it can be seen in Fig 6, the force linearly increases until the load reaches the local damage initiation point. The load nonlinearity increases until the crack initiation process is completed. Then, the crack tip starts propagating.

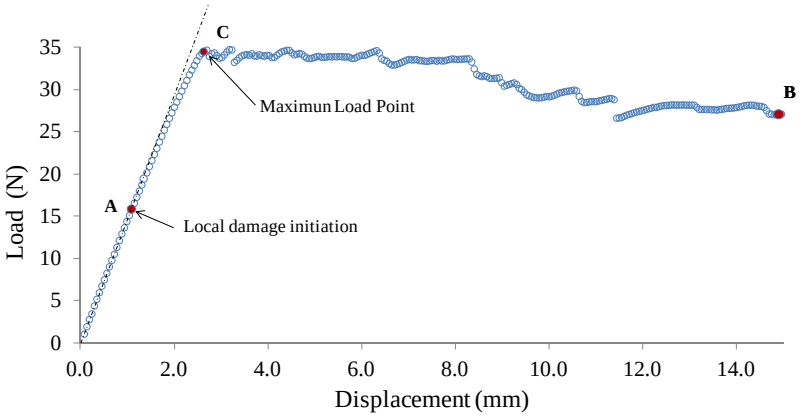

Figure 6: Load-Displacement experimental curve of specimen S1

After determining the crack length at each point of the test equating Eq (10) to the experimental compliance, the initial crack length is determined as an average value in the load range where the crack length remains constant as it can be seen in Fig 7. Therefore, the point where the local damage initiation occurs (point A) is related to the first point where the crack advance is not zero.

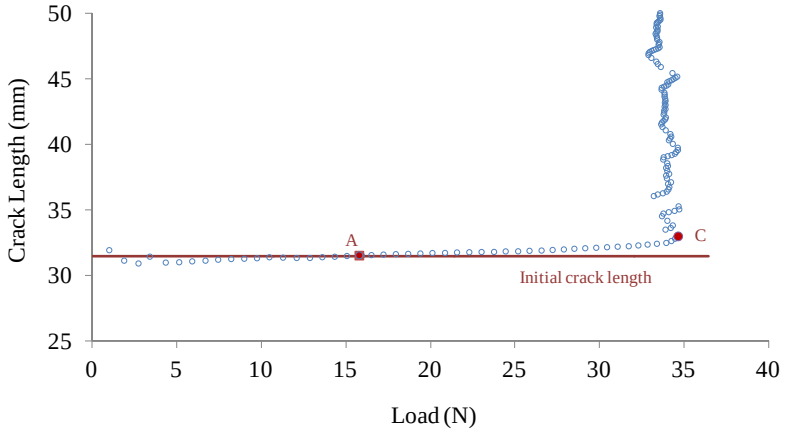

Figure 7: Crack length-load curves of specimen S1

Having the initial crack length and the crack length at each point of the test, it is possible to obtain the R-curves, which shows the evolution of *G* with respect to the crack advance, as shown in Fig. 8.

The initial rising trend of the G corresponding to the formation of FPZ (A-C) is followed by a region where the self-similar crack growth takes place (C-B). It can be seen that *G* increases as the crack propagates. This effect can be due to fiber bridging effect [22, 44, 45]. Therefore the last point of the test (B) is marked in Fig.8 and the corresponding value is denoted as G_B.

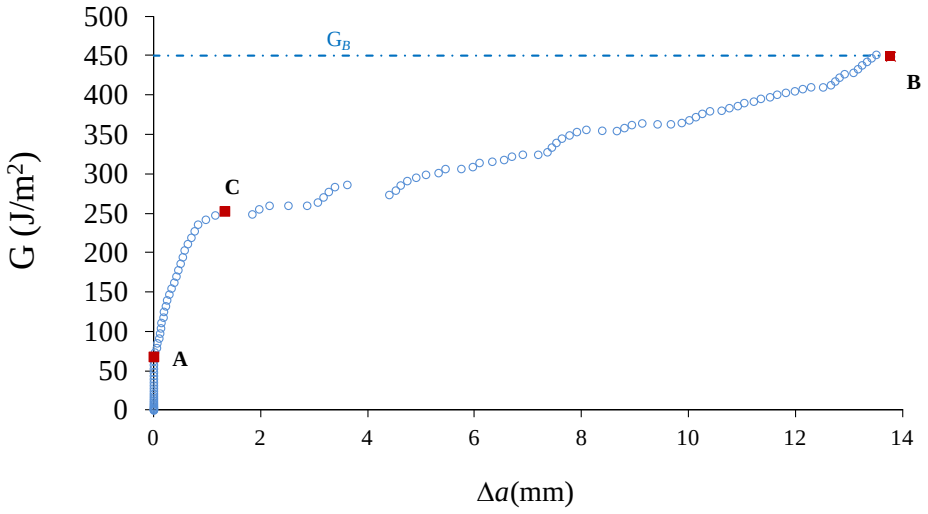

Figure 8: R curve in specimen S1

According to Eq. (12) the crack tip opening displacements can be determined at each point of the test, replacing the corresponding crack advance. Fig. 9 shows the G-Δ_n curve that corresponds to specimen S1.

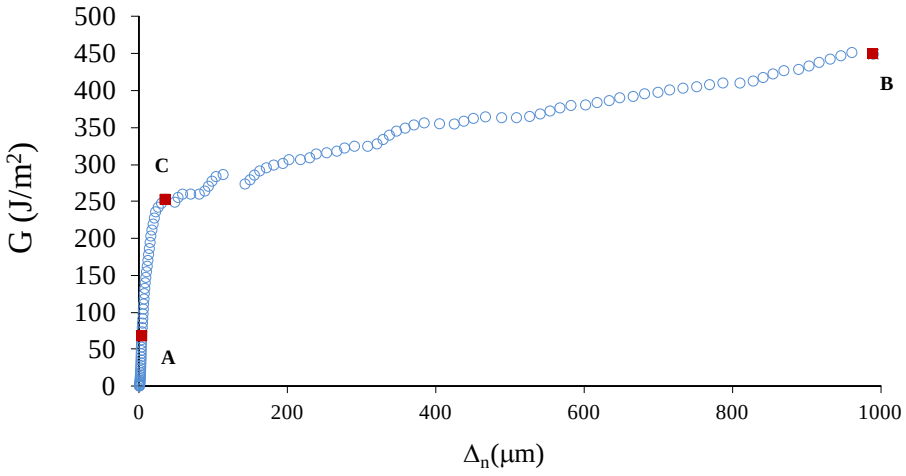

Figure 9: Relationship between the crack tip relative displacement Δ_n and the energy release rate *G* of specimen S1

In order to avoid the excessive noise of experimental data, G- Δ_n data is approached to the logistic function of Eq (13). $F(\Delta_n)$ function is fitted to experimental data by linear regional fitting. Fig. 10a shows the experimental data obtained from Eq. (13) and the fitted curve. In order to evaluate the accuracy of the fitting, the experimental data and the logistic function approach are plotted in Fig 10b.

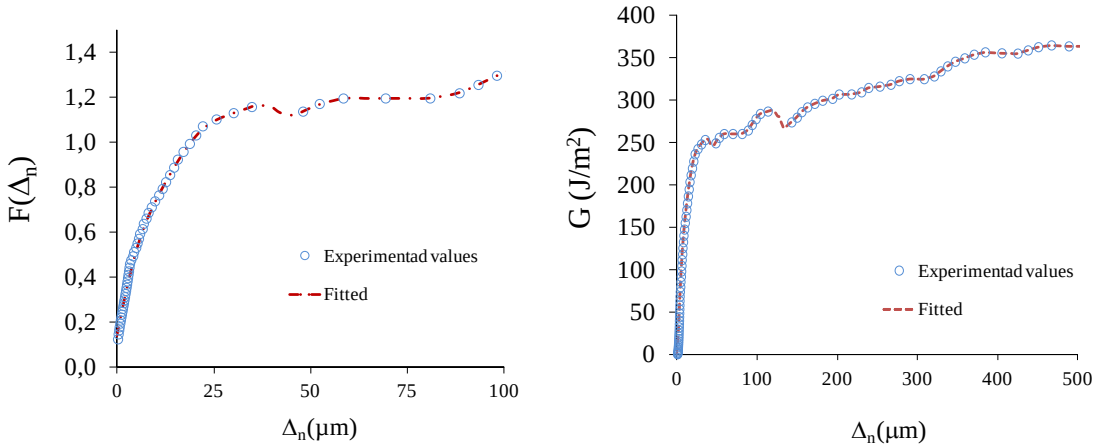

Figure 10: Experimental and fitted values of specimen S1: a/ $F(\Delta_n)$- Δ_n curve; b/ G-Δ_n curve.

Replacing the values of the fitted $F(\Delta_n)$ and its derivatives obtained by numerical differentiation in Eq (14), the cohesive law is obtained using the experimental data of load and displacement obtained from the testing machine.

Fig 11 shows the cohesive law of the specimen S1. The left figure shows the determined cohesive law for a wide range of crack opening displacements, while in the right figure the cohesive law is plotted for the initial crack opening displacement range.

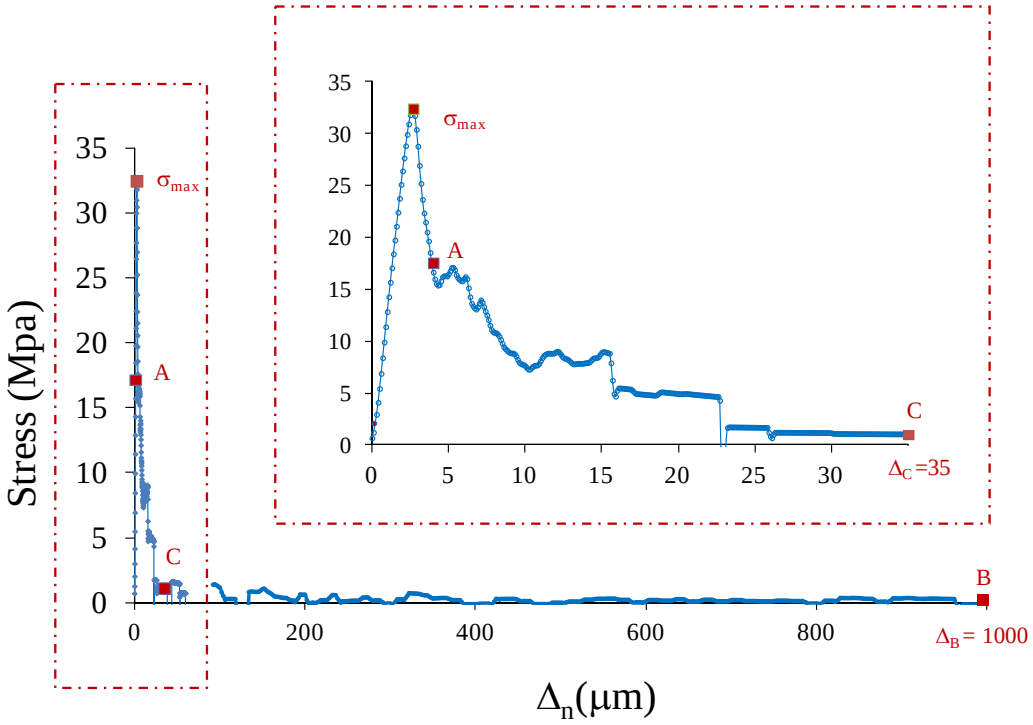

Figure 11: Cohesive law of the specimen S1

Different parts can be identified in the cohesive law (Fig 11): linear elastic behavior, damage initiation, de-cohesion and fiber bridging. [46, 47]

1. **Linear elastic behavior:** Initially, before any damage occurs, the behavior is close to linear elastic. The initial penalty stiffness can be determined as follows [46]:

$$k_p = \frac{\sigma_{max}}{\Delta_0}$$

where Δ_0 is the crack tip displacement to σ_{max}.

2. **Damage initiation:** The point A, defined as the point where the crack advance occurs, is assumed as the point where the damage starts. The crack tip displacement for this point is denoted as Δ_A, the stress σ_A and the value of G corresponding to this point is assumed as the damage initiation Energy Release Rate denoted as G^i_{IC}.
3. **De-cohesion:** On the other hand, the crack tip displacement for the maximum load point C is assumed as the point where de-cohesion takes place and it is denoted as Δ_C, which is the critical displacement point where a new crack surface is created. Δa_C is

assumed as the small scale cohesive fracture zones length (L_{FPZ_C}) [23, 48]. The value of G at this point is the propagation Energy Release Rate denoted as G^{p}_{IC}.

4. **Fiber bridging:** Finally in the wake of crack growing, fiber bridging occurs and this process increases the total fracture energy significantly. As it can be seen in Fig 11, the bridging stress is very low and the associated bridging zone is a large scale fracture zone. A mean value of that stresses named σ_B can be determined by the slope of the G-Δ_n curve between points C and B in Fig. 9 [19].

The most relevant values determined for the specimen S1 are summarized in table 1. It is worth noting that G increases significantly between C and B in spite of the low value of σ_B.

Δ_o (μm)	σ_{max} (MPa)	k_p (kN/mm^3)	σ_A (MPa)	G^i_{IC} (J/m^2)	Δ_C (μm)	L_{FPZ_C} (mm)	G^p_{IC} (J/m^2)	σ_B (MPa)	G_B (J/m^2)
2.7	32.4	12.0	17.6	48.4	35	1.33	252.9	0.2	450

Table 1 Results for the specimen S1

The penalty stiffness of the cohesive law must be equal to the tensile stiffness of the elastic foundation $k_p=k_e/b=2E_3/h$. In the present study the nominal value of the penalty stiffness obtained with k_e is 10.6 kN/mm^2. On the other hand, according to the data obtained from the cohesive law of Fig. 11 the penalty stiffness of specimen S1 is 12 kN/mm^3.

Regarding the prediction of maximum traction, according to Sorensen et al. [47] it should be equal to the transverse tensile strength of a transversely isotropic unidirectional composite, which in this case is 55 MPa.

In Fig. 11 it can be seen that σ_A corresponds to the transition stress in the softening law. Furthermore, the area of the cohesive law for the transition point represents G^i_{IC} [46, 47].

In order to check the applicability of the proposed data reduction method and its suitability to obtain the cohesive law in composite materials, 4 different specimens with 4 different initial crack lengths have been tested. Results have been obtained from the initial pre-cracked specimens. The nominal initial crack lengths of the specimens were:

S1: 30 mm; S2: 45 mm; S3: 40 mm; S4: 50 mm

The cohesive laws of the specimens are shown in Figure 12. The parameters explained previously are presented in Table 2.

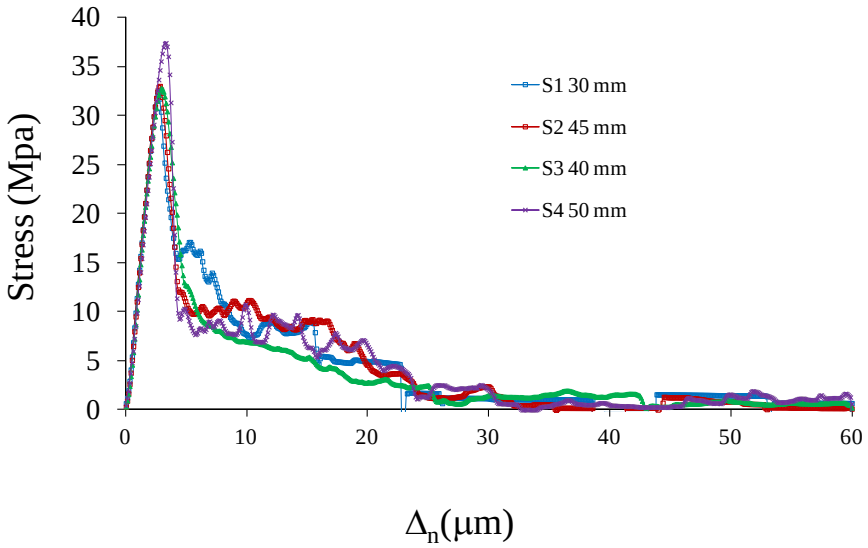

Figure 12: Cohesive law of S1, S2, S3 and S4 specimens

The most relevant values determined are shown in Table 2.

	Δ_o (μm)	σ_{max} *(MPa)*	k_p (kN/mm^3)	σ_A (MPa)	G^i_{IC} *(J/m^2)*	Δ_C *(μm)*	L_{FPZ_C} *(mm)*	G^p_{IC} *(J/m^2)*	σ_B (MPa)	G_B *(J/m^2)*
S1	2.7	32.4	12.0	17.6	73.7	35	1.33	252.9	0.21	450
S3	2.9	32.8	11.3	17.2	96.5	62	2.42	245.8	0.22	434

S2	2.8	33.0	11.8	14.6	84.1	46	1.79	256.4	0.15	377
S4	3.3	37.5	11.4	11.3	95.0	62	2.29	271.6	0.11	357
Mean	2.9	33.9	11.6	15.2	87.3	51.3	2.0	256.7	0.17	404.5
SD	±0.3	± 2.4	±0.3	±2.9	±10.6	±13.2	±0.5	±10.9	± 0.05	±44.5

Table 2 Results of S1, S2 S3 and S4 specimens

4. SUMMARY AND CONCLUSIONS

In the present paper, a new method for the determination of mode I cohesive law for unidirectional composite is proposed. The approach is based on the correlation between the developed Energy Release Rate (G) as a function of crack tip opening displacement (Δ_n). The Resistance Curve are determined obtaining the G as a function of the crack advance based on the compliance variation of the specimen as crack advances. The crack tip opening displacement is determined as a function of the equivalent crack advance assuming that the Fracture Process Zone development is analogous to an equivalent crack advance, related to the compliance variation. These measurements are used to compute the Energy Release Rate and crack opening displacement. A logistic function is fitted to the G-Δ_n curve and the experimental cohesive law is determined by numerical differentiation.

Experiments performed on a carbon/epoxy material are evaluated using the proposed method. The initiation G^i_{IC}, the critical G^p_{IC} and the cohesive strength obtained are in the order of 86 J/m^2, 256 J/m^2 and 34 MPa, respectively.

The proposed method provides a simple way to obtain the mode I cohesive law using only load-displacement data provided by the universal testing machine, without the need of any external displacement measurement and without assuming the shape of the cohesive law.

REFERENCES

[1] Hashemi S, Kinlochy AJ, Williams JG. Corrections needed in double-cantilever beam tests for assessing the interlaminar failure of fibre-composites. J Mater Sci Lett 1989; 8:125–29.

[2] Yoshihara H, Kawamura T. Mode I fracture toughness estimation of wood by DCB test. Compos Part A 2006; 37:2105–13.

[3] De Moura MFSF, Morais JJL, Dourado N. A new data reduction scheme for mode I wood fracture characterization using the double cantilever beam test. Eng Fract Mech 2008; 75:3852–65.

[4] De Moura MFSF, Campilho RDSG, Gonçalves JPM. Crack equivalent concept applied to the fracture characterization of bonded joints under pure mode I loading. Compos Sci Technol 2008; 68:2224–30.

[5] De Moura MFSF, Campilho RDSG, Amaro AM, Reis PNB. Interlaminar and intralaminar fracture characterization of composites. Compos Struct 2010; 92:144–9.

[6] Morais JJL, De Moura MFSF, Pereira FAM, Xavier J, Dourado N, Dias MIR. The double cantilever beam test applied to mode I fracture characterization of cortical bone tissue. J Mech Behavior Biomed Mater 2010; 3:446–53.

[7] Rybicki EF, Kanninen MF. A finite element calculation of stress intensity factors by a modified crack closure integral. Eng Fract Mech 1977; 9(4):931–8.

[8] Barenblatt, GI. Mathematical Theory of Equilibrium Cracks in Brittle Fracture. Adv Appl Mech 1962; 7: 55-129.

[9] Dugdale DS, Yielding of steel sheets containing slits 1960. Mech. Phys. Solids 8, 100–4.

[10] Shet C, Chandra N. Effect of the Shape of T–δ Cohesive Zone Curves on the Fracture Response. Mech Adv Mater Struc 2004; 11, 249-275.

[11] Hogberg JL, Sørensen BF, Stigh U. Constitutive behaviour of mixed mode loaded adhesive layer. Inter J Sol Struct 2007; 44 8335–54.

[12] Leffler, K, Alfredsson, KS, Stigh U. Shear behaviour of adhesive layers. Int. J. Sol Str 2007; 44: 530- 45.

[13] Sarrado C, Turon A, Costa J, Renart J, An experimental analysis of the fracture behavior of composite bonded joints in terms of cohesive laws. Compos Part A 2016; 90: 234–42.

[14] Soto A, González E, Maimí P, Turon A, Sainz de Aja JR, de la Escalera FM. Cohesive zone length of orthotropic materials undergoing delamination. Eng Fract Mech 2016; 159: 174– 88.

[15] Andersson T, Stigh U. The stress–elongation relation for an adhesive layer loaded in peel using equilibrium of energetic force. Int. J. Sol Str 2004; 41: 413–434.

[16] Ji G , Ouyang Z, Li G, Ibekwe S, Pang Su-Seng. Effect of adhesive thickenss on global and local Mode I interfacial fracture of bonded joints. Inter J Sol Str 2010; 47:2445-2458.

[17] Ji G , Ouyang Z, Li G,. Effects of bondline thickness on Mode-I nonlinear interfacial fracture of laminated composites: An experimental study. Compos Part B 2013; 47: 1–7.

[18] Sørensen BF, Kirkegaard P. Determination of mixed mode cohesive laws. Eng Fract Mech 2006; 73: 2642–2661.

[19] Sorensen BF, Jacobsen TK. Characterizing delamination of fibre composites by mixed mode cohesive laws. Compos Sci Technol 2009; 69: 445–456.

[20] de Morais A., Pereira AB. Application of the effective crack method to mode I and mode II interlaminar fracture of carbon/epoxy unidirectional laminates. Compos Part A 2007; 38: 785–794.

[21] Svensson D., Alfredsson K.S., Biel A., Stigh U. Measurement of cohesive laws for interlaminar failure of CFRP Compos Sci Technol 2014; 100: 53–62.

[22] Shokrieh M.M., Salamat-talab M., Heidari-Rarani M. M. Effect of initial crack length on the measured bridging law of unidirectional E-glass/epoxy double cantilever beam specimens. Materials and Design 55 (2014) 605–611.

[23] Shokrieh M.M., Salamat-talab M., Heidari-Rarani M. M. Dependency of bridging traction of DCB composite specimen on interface fiber angle. Theoretical and Applied Fracture Mechanics (2017) http://dx.doi.org/10.1016/j.tafmec.2017.02.009

[24] De Gracia J., Boyano A., Arrese A., Mujika F. A new approach for determining the R-curve in DCB tests without optical measurements Engineering Fracture Mechanics 135 (2015) 274–285

[25] Rice JR. A path independent integral and the approximate analysis of strain concentration by notches and cracks. J Appl Mech 1968;35:379–86.

[26] Suo, Z., Bao, G., Fan, B., 1992. Delamination R-curve phenomena due to damage. Journal of the Mechanics and Physics of Solids 40, 1–16.

[27] Anderson TL. Fracture Mechanics. Fundamentals and applications. 2005.

[28] Sorensen B.F, Jacobsen T.K. Determination of cohesive laws by the J integral approach. Engineering Fracture Mechanics 70 (2003) 1841–1858.

[29] Boyano A, Mollón V, Bonhomme J, De Gracia J, Arrese A, Mujika F. Analytical and numerical approach of an End Notched Flexure test configuration with an inserted roller for promoting mixed mode I/II. Eng Fract Mech 2015;143:63–79.

[30] Sørensen BF,Jacobsen TK Large-scale bridging in composites: R-curves and bridging laws. Composites Part A: Volume 29, Issue 11, November 1998, Pages 1443-1451.

[31] ASTM. «Standard D5528-94a, standard test method for mode I interlaminar fracture toughness of unidirectional continuous fiber reinforced polymer matrix composites», Philadelphia; 1994.

[32] Williams JG. End corrections for orthotropic DCB specimens. Compos Sci Technol 1989;35(4):367–76.

[33] Kanninen MF. A dynamic analysis of unstable crack propagation and arrest in the DCB test specimen. Int J Fract 1974;10(3):415–30.

[34] Kanninen MF. An augmented double cantilever beam model for studying crack propagation and arrest. Int J Fract 1971;9(1):83–92.

[35] Whitney JM. Stress analysis of the double cantilever beam specimen. Compos Sci Technol 1985;23:201–19.

[36] Brunoy D, Greco F. Mixed mode delamination in plates: a refined approach. Int J Solids Struct 2001;38:9149–77.

[37] Olsson R. A simplified improved beam analysis of the DCB specimen. Compos Sci Technol 1992;43:329–38.

[38] Ozdily F, Carlsson L. Beam analysis of angle-ply laminate DCB specimens. Compos Sci Technol 1999;59:305–15.

[39] Kondo K. Analysis of double cantilever beam specimen. Adv Compos Mater 1995;4(4):355–66.

[40] Oden JT, Ripperger EA. Mechanics of elastic structures. 1981:460.

[41] Silva F.G.A, Morais J.J.L., Dourado N., Xavier J., Pereira F.A.M., de Moura M.F.S.F. Determination of cohesive laws in wood bonded joints under mode II loading using the ENF test. International JournalofAdhesion&Adhesives51(2014)54–61

[42] Data curve fit creator Add in V262, SRS1 Software LLC, Boston, Massachusetts, United States of America. www.srs1software.com

[43] Mujika F. On the effect of shear and local deformationin three point bending tests. Polymer testing 2007;26:869-77

[44] Tamuzs V, Tarasovs S, Vilks U. Progressive delamination and fiber bridging modeling in double cantilever beam composite specimens. Eng Fract Mech 2001;68(5):513–25.

[45] Szekrényes A. Advanced beam model for fiber-bridging in unidirectional composite double-cantilever beam specimens. Eng Fract Mech 2005;72(17):2686–702.

[46] Heidari-Rarani M., Shokrieh M.M., Camanho P.P., Finite element modeling of mode I delamination growth in laminated DCB specimens with R-curve effects. . Compos Part B 45 (2013) 897–903

[47] Sorensen L., Botsis J., Gmür Th., Humbert L. Bridging tractions in mode I delamination: Measurements and simulation. Composites Science and Technology 68 (2008) 2350-2358.

[48] Bergan A, Dávila, C, Leoné F Awerbuch J, Tan TM. A mode I cohesive law characterization procedure for thought the thickness crack propagation in composite laminates. . Compos Part B 94 (2016) 338-349